Fluctuation-induced currents in suspended graphene nanoribbons: Adiabatic quantum pumping approach

Federico D. Ribetto [1,2] Silvina A. Elaskar [3] Hernán L. Calvo [1] and Raúl A. Bustos-Marún [1,3,*]

[1]*Instituto de Física Enrique Gaviola (CONICET) and FaMAF, Universidad Nacional de Córdoba, X5000HUA, Argentina*
[2]*Departamento de Física, Universidad Nacional de Río Cuarto, Río Cuarto, X5804BYA, Argentina*
[3]*Facultad de Ciencias Químicas, Universidad Nacional de Córdoba, X5000HUA, Argentina*

Graphene nanoribbons (GNRs) are thin strips of graphene with unique properties due to their structure and nanometric dimensions. They stand out as basic components for the construction of different types of nanoelectromechanical systems (NEMS), including some very promising sensors and pumps. However, various phenomena, such as unintended mechanical vibrations, can induce undesired electrical currents in these devices. Here, we take a quantum mechanical approach to analyze how currents induced by fluctuations (either thermal or of some other kind) in suspended GNRs contribute to the electric current. In particular, we study the pumping current induced by the adiabatic variation of the Hamiltonian of the system when a transverse vibration (flexural mode) of a GNR suspended over a gate is excited. Our theoretical approach and results provide useful tools and rules of thumb to understand and control the charge current induced by fluctuations in GNR-based NEMS, which is important for their applications in nanoscale sensors, pumps, and energy harvesting devices.

I. INTRODUCTION

Being one of the strongest materials ever tested [1] with large thermal and electrical conductivities [2,3], graphene and, in particular, the more tunable graphene nanoribbons (GNRs) have become the conductive building blocks of innumerable nanoelectromechanical systems (NEMSs). GNR-based NEMSs have been studied as electromechanical resonators [4–7]; electron pumps [8–14]; sensors of mass, pressure, strain, and temperature [15–17], as well as detectors of vibrations [18] and gases [19]; switches [20]; ultrasmall accelerometers [21]; and even viral detectors for COVID-19 [22].

In all of the above examples, it is essential to study the various phenomena that can limit the use of the proposed devices, such as the noise in electrical currents. Besides the thermal (or Nyquist-Johnson) noise [23,24], other phenomena can also interfere with the detected electrical currents. For example, suspended GNRs are in constant mechanical motion at room temperature, which can induce measurable oscillations in the electrical current, as recently shown [25]. Of course, oscillations are not only due to thermal excitations and other phenomena, such as the propagation of vibrational waves through the material, which can also cause them.

Typically, the calculations of instantaneous electric currents induced by vibrations are based on classical models of time-dependent capacitances [25]. Here, instead, we adopt a quantum mechanical approach to this problem and analyze the contributions to the current due to the adiabatic

quantum pumping [26–28] arising from the stochastic oscillation of GNRs. Quantum pumping currents are a consequence of the delayed response of electronic wave functions to a time-dependent Hamiltonian which, in the present case, originates from the movement of the nuclei. In this regard, a comment is in order to avoid confusions. Since the oscillations of individual vibrational modes are independent, the generation of pumping currents produced by them is expected to average to zero over a period. This is because, to have a finite pumped charge per cycle, more than one time-dependent parameter needs to be moved with a fixed phase [26]. However, even if the pumping currents have a null mean value, this does not prevent them from contributing instantaneously to the total current and, thus, to the current noise, when the Hamiltonian parameters move stochastically. This crucial point marks a clear difference with some previous works, e.g., Refs. [10,12–14]. While there the authors studied the pumped charge in GNRs (meaning the average dc current per cycle), here we are interested in the maximum value of the instantaneous adiabatic pumping currents induced by stochastic fluctuations of GNRs.

In particular, we study a common configuration of GNR-based NEMSs consisting of a GNR suspended over a controllable gate, see Fig. 1(a). There, we evaluate the contribution to the electric current due to quantum pumping induced by the movement of the lowest frequency (acoustic) modes for the transversal vibration of suspended GNRs, also known as flexural modes [12]; see Figs. 1(b) and 1(c). To this end, we adapted the theoretical description of adiabatic quantum pumping [26] to the generic case of vibrational normal modes [28]. Our methodology and results are not only relevant for different types of sensors and pumps based on GNRs, but they can also be extended to other applications such as energy

*rbustos@famaf.unc.edu.ar
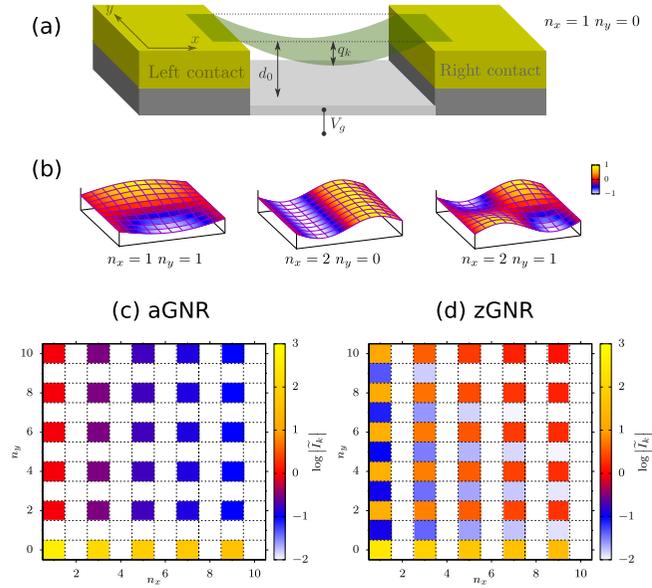
FIG. 1. (a) Scheme of the studied system: A suspended GNR between two metallic contacts freely oscillating, at a distance d_0, over a gate with gate voltage V_g. We only consider the lowest frequency (acoustic) modes for the transversal vibration of the GNRs in a classical approximation and assume a rectangular membrane model to describe them. The shown mode corresponds to $(n_x, n_y) = (1, 0)$. (b) Other examples of normal modes with (from left to right): $(n_x, n_y) = (1, 1), (2, 0),$ and $(2, 1)$. (c), (d) Logarithm of the scaled emissivity $\tilde{I}_k$ in the low-temperature limit as a function of n_x and n_y for square nanoribbons with armchair (aGNR) and zigzag (zGNR) edges. $\tilde{I}_k$ has units of $1/eV$ and is proportional to the maximum value of the pumping current during a period. The size of the ribbons is $L = 449\,a$ (with $a = 0.246\,nm$) and the Fermi energy is $\varepsilon_F = 0.1\,eV$.

FIG. 2. Examples of GNRs with zigzag (zGNR) and armchair (aGNR) edges (blue and orange sites) connected to two semi-infinite contacts on the left and right (red sites). Note that the contacts are also made of GNRs of the same width and type. The green rectangles show how a row is defined for each type of GNR (to be used in Sec. III B).

harvesting at the nanoscale [25,28,29] or to other systems such as carbon nanotubes.

The paper is organized as follows. In Sec. II, we present the theoretical framework, including the different models and approximations used in our calculations. In Sec. III, we explore the role of different system parameters on the fluctuation-induced currents, including the length, type of border, and Fermi energy of GNRs. At the end of this section, we also present a realistic estimation of the expected value of currents. In Sec. IV, we develop a semiclassical theory to evaluate the zero-frequency noise of thermally induced pumping current and use it to compare with Nyquist-Johnson zero-frequency noise. Finally, in Sec. V we summarize and discuss the main results.

II. THEORETICAL FRAMEWORK

Due to the vast number of variables that can potentially influence the current induced by the oscillations of GNRs, throughout the paper we focus on certain limits, approximations, and simplified models that allow us to obtain simple expressions that nonetheless can be used to understand the general features of the studied phenomenon.

A. GNR: Electronic modeling

1. Hamiltonian

Considering energies close to the Fermi energy, the description of the electrons in graphene can be carried out by means of a tight-binding model [30]. Given the energy difference between the σ and π molecular orbitals, and the fact that the band of π orbitals is the one found around the Fermi energy, we will only consider p_z atomic orbitals. Thus, we have the following Hamiltonian:

$$\hat{H} = \sum_i \varepsilon_i \hat{c}_i^\dagger \hat{c}_i - \sum_{\langle i,j \rangle} t_{i,j} \hat{c}_i^\dagger \hat{c}_j, \tag{1}$$

where ε_i is the energy of site i, $\hat{c}_i^\dagger$ and $\hat{c}_i$ are the creation and annihilation operators in the p_z orbital of site i, and $t_{i,j}$ represents the hopping amplitude between sites i and j. Furthermore, the sum $\langle i, j \rangle$ is restricted to nearest-neighbor sites. In the absence of defects and external disturbances, ε_i is set to zero for simplicity, while the bare hopping amplitude takes the value $t_{i,j} \equiv t_0 = 2.66\,eV$ [30].

2. Electronic properties

Graphene nanoribbons are usually cuts in a certain direction. Based on the direction of the cut, typically two edge types are described: the *zigzag* edge [Fig. 2(a)] and *armchair* edge [Fig. 2(b)]. To classify the ribbons, the following convention will be used: GNRs with armchair (zigzag) edges are classified by the number of dimer lines (zigzag lines) across the width of the ribbon. In addition, the notation N-aGNR (N-zGNR) will be used for armchair (zigzag) GNRs, where N is the number of dimer lines (zigzag lines) [30].

N-aGNR and N-zGNR have very different electronic properties that arise from their contrasting boundary conditions. Some aGNR exhibit semiconductor behavior, while others are metallic. An analytical calculation of the eigenvalues of the tight-binding Hamiltonian allows us to show that the energy

gap Δ_N of N-aGNR oscillates with the width of the ribbon [31] besides the obvious decaying limit $\Delta_N \to 0$ for $N \to \infty$. In particular, we have that $\Delta_N = 0$ for $N = 3\ell + 2$, where ℓ is an integer, making it metallic or semiconducting otherwise [30,32].

Unlike the previous case, the zGNRs retain the semimetallic character of graphene, regardless of their width. Another interesting feature is the formation of a pronounced peak in the density of states for $\varepsilon = 0$, which results from the formation of partially flat and degenerate bands with zero energy [30]. The presence of these highly confined electronic edge states has been confirmed by scanning tunneling microscopy and spectroscopy [30]. They have a topological protection that makes them robust against different types of disturbances such as vacancies or Anderson-type noise [30,33].

3. System and contacts

In our calculations, we will assume the configurations shown in Fig. 2 of the system depicted in Fig. 1(a). There, we define a finite central region (blue and orange dots in Fig. 2) that is able to oscillate and is coupled to two semi-infinite and identical contacts, left (L) and right (R) (red dots), that are also made of GNRs of the same type as that of the central region.

B. GNR: Oscillating membrane model

We are going to assume that the GNRs are large enough to be able to approximate its transversal normal modes of vibration by those of a rectangular membrane (limit of the continuum for low-frequency acoustic modes). We also assume that this membrane is placed in the xy plane, and $z(x, y, t)$ is a function that describes its displacement with respect to said plane, see Fig. 1(a). Consequently, the equation that governs the transverse movement of the membrane is (see Appendix A for more details)

$$z(x, y, t) = \sum_{n_x,n_y=0}^{\infty} \sin\left(\frac{n_x \pi}{L_x} x\right) \cos\left(\frac{n_y \pi}{L_y} y\right) q_{n_x,n_y}, \quad (2)$$

where L_x and L_y are the length and width of the central region, respectively, and the amplitude of the mode q_{n_x,n_y} (defined by the pair of integers $n_x = 1, 2, ...$ and $n_y = 0, 1, ...$) is

$$q_{n_x,n_y} \equiv A_{n_x,n_y} \cos(\omega_{n_x,n_y} t + \phi_{n_x,n_y}). \quad (3)$$

Figure 1(b) shows some examples of modes for different pairs (n_x, n_y). In the above equation, the phase ϕ_{n_x,n_y} of the oscillation is arbitrary, the maximum amplitude of q will be discussed afterwards, and the frequencies of the normal modes are given by

$$\omega_{n_x,n_y} = v \sqrt{\left(\frac{n_x \pi}{L_x}\right)^2 + \left(\frac{n_y \pi}{L_y}\right)^2}, \quad (4)$$

where v is the speed of sound in graphene (for low-frequency transversal acoustic waves). For simplicity, from now on we will collapse the pair of indices n_x and n_y into a single one k. A central quantity that will be needed in our calculations is the maximum velocity of the normal modes, given by

$$\dot{q}_{k,\max} = A_k \omega_k. \quad (5)$$

The energy associated with the normal modes of graphene, see Appendix B, can be written as

$$E_k = m_c\left(\tfrac{1}{2}\dot{q}_k^2 + \tfrac{1}{2}\omega_k^2 q_k^2\right) = \tfrac{1}{2}m_c A_k^2 \omega_k^2, \quad (6)$$

where m_c is the mass of a carbon atom. Now we can use equipartition theorem together with the above equation to derive an estimation for A_k, which yields

$$A_k = \frac{1}{\omega_k}\sqrt{\frac{2k_B T}{m_c}}. \quad (7)$$

As we will see in Eq. (11), the above expression implies that the maximum value of the pumping current is independent of the frequency of the mode.

C. Quantum pumping current

The objective of this section is to derive an expression that allows us to calculate the maximum value of the pumping current on the reservoir r, $I_{r,k,\max}^{(1)} \equiv \max[I_{r,k}^{(1)}(t)]$, over a period of oscillation of a given normal mode k of a suspended GNR. This pumping current, typically denoted with a superscript (1), is associated with the first order term of an adiabatic expansion of the observable current, and arises from the delayed electronic response of the system to the time variation of some classical parameters; see Appendix C. It has been thoroughly studied by using different formalisms [26,34,35] and in a variety contexts (even outside quantum transport [36]) but only as a way of generating dc currents controlled by the movement of at least two systems' parameters.

Since our interest here lies in stochastic variations of the system's parameters (the vibrational normal modes q_k), it is necessary to highlight that the associated pumping currents average to zero in one period of $q_k(t)$. However, this does not mean that $I_{r,k}^{(1)}(t)$ is always zero. On the contrary, vibration-induced currents can instantaneously (at a given time) contribute to the total current which, as discussed in the Introduction, can potentially interfere with current measurements in sensors based on GNRs, for example.

We will work under a perturbative limit of the modes, i.e., small amplitudes of the oscillation, and thus $\mathbf{q}(t) \approx \mathbf{q}_0$, where $\mathbf{q}$ is the vector containing the amplitudes q_k of all normal modes, and $\mathbf{q}_0 \equiv \mathbf{0}$ is the equilibrium position of the system.[1] Therefore, we can approximate $I_r^{(1)}(t)$ as

$$I_r^{(1)}(t) = e\sum_k \frac{dn_r(\mathbf{q})}{dq_k}\dot{q}_k(t) \approx e\sum_k \left(\frac{dn_r}{dq_k}\right)_{\mathbf{q}_0}\dot{q}_k(t), \quad (8)$$

where $(dn_r/dq_k)_{\mathbf{q}_0}$ is the emissivity due to the kth normal mode evaluated at $\mathbf{q}_0$. This emissivity can be written in terms of the scattering matrix S of the system as [26]

$$\left(\frac{dn_r}{dq_k}\right)_{\mathbf{q}_0} = \int \frac{d\epsilon}{2\pi}\left(-\frac{\partial f}{\partial \epsilon}\right) \sum_{\alpha \in r, \beta} \text{Im}\left[\frac{\partial S_{\alpha\beta}}{\partial q_k} S_{\alpha\beta}^*\right]_{\mathbf{q}_0}, \quad (9)$$

where f is the equilibrium Fermi function (we are assuming a zero bias voltage configuration), α and β are channel indices

---

[1] In our model, the equilibrium position (no excitation of vibrational modes for the oscillation of GNRs) corresponds to a flat still membrane, equivalent to setting $\mathbf{q}_0 = \mathbf{0}$.

of the contacts, and we require $\alpha \in r$, since we want to calculate the emissivity at contact r to determine the associated quantum pumping current $I_r^{(1)}$. If we additionally take the limit of low temperatures, Eq. (9) reduces to

$$
\left(\frac{dn_r}{dq_k}\right)_{\varepsilon_F, \boldsymbol{q}_0} = \sum_{\alpha \in r, \beta} \frac{1}{2\pi} \text{Im}\left[\frac{\partial S_{\alpha\beta}}{\partial q_k} S_{\alpha\beta}^*\right]_{\varepsilon_F, \boldsymbol{q}_0}. \quad (10)
$$

It is interesting to note that the above equation holds even at finite temperatures if the right-hand side of Eq. (9) depends linearly on the energy around ε_F. Due to the approximation used, emissivities do not depend on time. Then, the maximum value of the kth contribution to the pumping current $I_{r,k}^{(1)}$ (defined through $I_r^{(1)}(t) = \sum_k I_{r,k}^{(1)}$) is simply

$$
I_{r,k,\text{max}}^{(1)} = \left|e\left(\frac{dn_r}{dq_k}\right)_{\varepsilon_F, \boldsymbol{q}_0} \dot{q}_{k,\text{max}}\right|, \quad (11)
$$

where $\dot{q}_{k,\text{max}}$ is the maximum value of $\dot{q}_k$.

D. Emissivities

The explicit expression of the emissivity depends on the Hamiltonian model used. Here, we assume small displacements in the direction perpendicular to the GNR plane, z. Thus, we can take a linear regime of the diagonal elements of the Hamiltonian,

$$
H_{ii} = E_0 + \left(\frac{\partial E}{\partial z}\right)\delta z_i, \quad (12)
$$

where $\delta z_i = [z_i(x_i, y_i, \boldsymbol{q}) - z_i(x_i, y_i, \boldsymbol{q}_0)]$, $E_0 = \varepsilon_i = 0$, and the factor $(\partial E/\partial z)$ is the same for all sites. Taking the limit of large sizes for the GNR, within which our model should behave like a classical parallel plate capacitor, it can be shown (see Appendix D) that this factor should satisfy the relation

$$
\left(\frac{\partial E}{\partial z}\right) = -\epsilon_0 \frac{A_{\text{site}} V_g^2}{d_0^2}, \quad (13)
$$

where A_{site} is the area associated with each individual site, V_g is the potential difference between the membrane and the gate (gate voltage), d_0 is the distance between the GNR and the gate, and ϵ_0 is the vacuum permittivity.

In GNRs, the hopping amplitudes in the Hamiltonian usually take an exponential dependence on the distance between first neighbors [37],

$$
t_{i,j} = t_0 e^{-b\left(\frac{|\boldsymbol{r}_i - \boldsymbol{r}_j|}{a_{\text{cc}}} - 1\right)}, \quad (14)
$$

where a_{cc} is the equilibrium distance between neighboring atoms and b is a constant that sets how much the hoppings change with the distance $|\boldsymbol{r}_i - \boldsymbol{r}_j|$. Here, the distance $|\boldsymbol{r}_i - \boldsymbol{r}_j|$ is a quantity that depends on the modes that are being excited and can be expressed as

$$
|\boldsymbol{r}_i - \boldsymbol{r}_j| = \sqrt{a_{\text{cc}}^2 + (\delta z_i - \delta z_j)^2}. \quad (15)
$$

Given that we are considering that the amplitude A_k of the modes is small, we can approximate

$$
t_{i,j} \approx t_0 \left[1 - \frac{b}{2}\left(\frac{\delta z_i - \delta z_j}{a_{\text{cc}}}\right)^2\right]. \quad (16)
$$

The Hamiltonian of the system can then be divided into two parts, $\boldsymbol{H} = \boldsymbol{H}^{(E)} + \boldsymbol{H}^{(V)}$, where $\boldsymbol{H}^{(E)}$ contains $\boldsymbol{H}(\boldsymbol{q}_0)$ and the site energies' dependence on $\boldsymbol{q}$,

$$
H_{ij}^{(E)} = \begin{cases} E_0 + \left(\frac{\partial E}{\partial z}\right)\delta z_i & i = j \\ -t_0 & i = j \pm 1, \end{cases} \quad (17)
$$

and $\boldsymbol{H}^{(V)}$ contains only the hoppings' dependence on $\boldsymbol{q}$:

$$
H_{ij}^{(V)} = \begin{cases} 0 & i = j \\ \dfrac{t_0 b}{2}\left(\dfrac{\delta z_i - \delta z_j}{a_{\text{cc}}}\right)^2 & i = j \pm 1. \end{cases} \quad (18)
$$

Then, using the Fisher-Lee formula, one can prove (see Appendix E) that the derivatives with respect to q_k of the scattering matrix can be decomposed into

$$
\frac{\partial \boldsymbol{S}}{\partial q_k} = \frac{\partial \boldsymbol{S}^{(E)}}{\partial q_k} + \frac{\partial \boldsymbol{S}^{(V)}}{\partial q_k}, \quad (19)
$$

where $\boldsymbol{S}^{(E)}$ and $\boldsymbol{S}^{(V)}$ are the scattering matrices obtained from Hamiltonians $\boldsymbol{H}^{(E)}$ and $\boldsymbol{H}^{(V)}$, respectively. It can be readily shown that, for small oscillations, $\partial \boldsymbol{S}^{(V)}/\partial q_k$ can be neglected, see Appendix E. Using this, and noting that $\boldsymbol{S}(\boldsymbol{q}_0) = \boldsymbol{S}^{(E)}(\boldsymbol{q}_0)$, the emissivity takes the form

$$
\left(\frac{dn_r}{dq_k}\right)_{\varepsilon_F, \boldsymbol{q}_0} \approx \left(\frac{dn_r^{(E)}}{dq_k}\right)_{\varepsilon_F, \boldsymbol{q}_0}, \quad (20)
$$

where $dn_r^{(E)}/dq_k$ is the emissivity calculated with Hamiltonian $\boldsymbol{H}^{(E)}$.

To simplify the analysis of the next sections, we define the *scaled* emissivity, which removes from $dn_r^{(E)}/dq_k$ the parameters related to particularities of the studied system, i.e.,

$$
\left(\frac{d\tilde{n}_r^{(E)}}{dq_k}\right) \equiv \left(-\epsilon_0 \frac{A_{\text{site}} V_g^2}{d_0^2}\right)^{-1}\left(\frac{dn_r^{(E)}}{dq_k}\right). \quad (21)
$$

Finally, the maximum value of the quantum pumping current, given by the oscillation of a mode q_k with energy $k_B T$, yields

$$
I_{r,k,\text{max}}^{(1)} = \left|\frac{e\epsilon_0 A_{\text{site}} V_g^2}{d_0^2}\sqrt{\frac{2k_B T}{m_c}}\left|\frac{d\tilde{n}_r^{(E)}}{dq_k}\right|_{\varepsilon_F, \boldsymbol{q}_0}\right|. \quad (22)
$$

This expression can be divided into three contributions: the first one from left to right is the scaling factor and it accounts for the gate voltage and the distance between the GNR and the gate; the second one is the amplitude factor and it accounts for the amplitude of the k mode oscillation (in this case given only by the temperature), and the last one is the scaled emissivity which is independent of the other quantities. To simplify the notation, from now on the scaled emissivity will be denoted as $\tilde{I}_k$, i.e.,

$$
\tilde{I}_k \equiv \left(\frac{d\tilde{n}_r^{(E)}}{dq_k}\right)_{\varepsilon_F, \boldsymbol{q}_0}, \quad (23)
$$

where we omitted the r subindex since it is irrelevant for the present case with equal contacts and zero bias voltage. This quantity, which has units of one over energy, can be transformed into a true current simply by multiplying it by the scaling and amplitude factors; see Eq. (22).
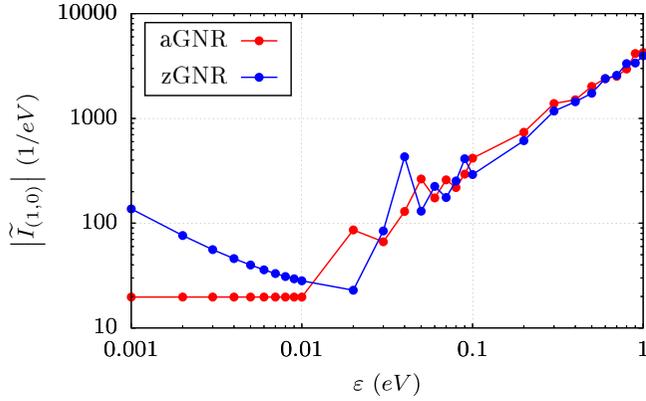
FIG. 3. Scaled emissivity $\tilde{I}_{(1,0)}$ in units of 1/eV, as a function of the Fermi energy ε_F for square GNRs with $L = 449\,a$.

III. PUMPING CURRENTS INDUCED BY OSCILLATIONS OF THE GNR

The main quantity to be discussed in Secs. III A, III B, and III C, and plotted in Figs. 1, 3–5, is the scaled emissivity $\tilde{I}_k$ in the low-temperature limit, where $\tilde{I}_k$ is proportional to the maximum value of the pumping current during a cycle of the k mode. In Secs. III A, III B, and III C we mainly study the dependence of $\tilde{I}_k$ on different characteristics of the GNRs, while in Sec. III D we discuss a realistic estimation of the maximum value of the vibration-induced pumping current in typical GNRs. To carry out these tasks, we use the theory and models previously presented, combining them with the numerical tools provided by the KWANT package [38] for the calculation of the scattering matrices. In the plots, all energies are in eV while distances are in units of $a \equiv \sqrt{3}a_{cc} = 0.246\,\text{nm}$, which is the length of the primitive vectors of the associated Bravais lattice [30].

A. Mode dependence

Here we study the effect of the mode oscillation on the quantum pumping current through the calculation of $\tilde{I}_k$ for
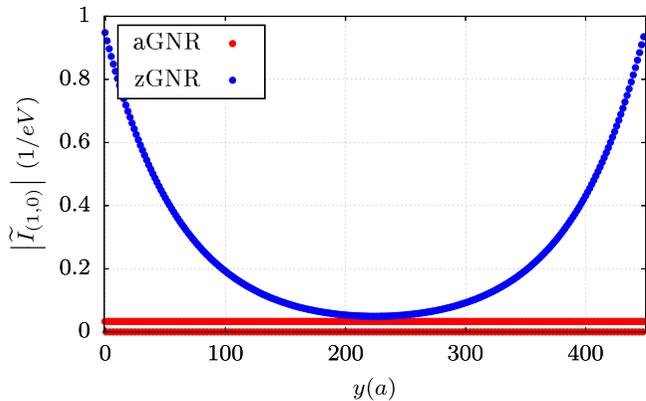
FIG. 4. Contribution of each row of atoms [calculated using Eq. (24)] to the scaled emissivity $\tilde{I}_{(1,0)}$, for square GNRs of side $L = 449\,a$, and $\varepsilon_F = 0.001$ eV. The value of y is the position of the row, in units of a. See Fig. 2 for examples of rows for each type of GNR.
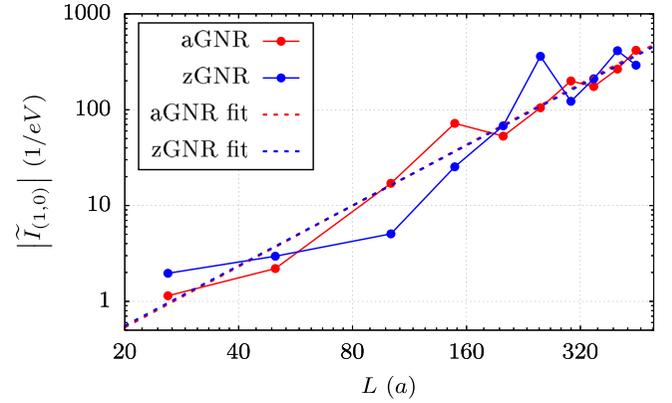
FIG. 5. Scaled emissivity $\tilde{I}_{(1,0)}$ as a function of the system's size L for square GNRs, with $\varepsilon_F = 0.1$ eV. The linear fits in dotted lines, show the approximate quadratic dependence between $\tilde{I}_{(1,0)}$ and L. $\tilde{I}_{(1,0)} = 10^{-2.01}L^{2.11}$ for aGNR and $\tilde{I}_{(1,0)} = 10^{-2.97}L^{2.09}$ for zGNRs.

different values of n_x (in the range [1,10]) and n_y (in the range [0,10]), taking into account both zigzag and armchair edges. For the calculations we consider, a square membrane with length L_x and width L_y equal to $449\,a \sim 0.1\,\mu$m. This value of L_y ensures that the aGNR is metallic (see Sec. II A 2) and that the system is large enough to validate the rectangular membrane model (Sec. II B). Regarding the Fermi energy, the value $\varepsilon_F = 0.1$ eV was taken, which ensures that we are working far from edge states for the zigzag case, which can cause the pumping current to diverge (see Sec. III B).

The dependence of $\tilde{I}_k$ on the excited mode is illustrated in Fig. 1(c) for armchair edges and in Fig. 1(d) for zigzag edges. It is clear, in both cases, a relationship between the symmetry of the normal modes and the pumping current: If n_x is even or if n_y is odd, the pumped current is negligible. This behavior can be explained by analyzing the contribution of each atom l to the total emissivity of a mode k, that is,

$$\left(\frac{d\tilde{n}_r}{dq_k}\right) = \sum_l \left(\frac{d\tilde{n}_r}{dz_l}\right)\frac{\partial z_l}{\partial q_k}, \tag{24}$$

where $(d\tilde{n}_r/dz_l)$ is the emissivity given by moving only atom l. If we now assume that the system is infinite and that all atoms are equivalent, in the sense that their variation equally affects the scattering matrix, we can write

$$\left(\frac{d\tilde{n}_r}{dq_k}\right) \approx \left(\frac{d\tilde{n}_r}{dz_l}\right)\sum_l \frac{\partial z_l}{\partial q_k}. \tag{25}$$

Then, based on this assumption, we see that it is only the position of each atom $[z_l \equiv z_l(x_l, y_l, \boldsymbol{q})]$ and the normal mode involved q_k which determines its contribution to the total current. Thus, for those vibrations where n_x is even or n_y is odd, any contribution to the pumping current is canceled by a contribution of the opposite sign. It is important to note that, even if the previous approximation is not completely valid (for example, due to the finite size of the system), it can still be expected in certain cases that the maximum value of the pumping current is zero. This occurs when the system presents a reflection symmetry with respect to a line that cuts the nanoribbon in half. In that case, for any pair of sites i and j in mirror positions with respect to a line parallel (or

perpendicular) to the direction of transport, the emissivities per atom must be equivalent, i.e.,

$$\left(\frac{d\tilde{n}_r}{dz_i}\right) = \left(\frac{d\tilde{n}_r}{dz_j}\right). \tag{26}$$

Given that for n_y odd (n_x even), the following relation holds:

$$\frac{\partial z_i}{\partial q_k} = -\frac{\partial z_j}{\partial q_k}, \tag{27}$$

it is clear that $\tilde{I}_k = 0$.

As can be seen in Fig. 1, the above arguments hold quite well for even n_x on both types of ribbons. This is reasonable considering that the system is truly infinite in the x direction. Let us recall that we are using as contacts semi-infinite nanoribbons of the same width and type as that of the suspended system. In this way, the pumping current is strictly zero for n_x even, when the positions of the equivalent atoms coincide exactly with a reflection with respect to a line perpendicular to the direction of transport that cuts the system in half. The deviations from this are very small for the values of L used and therefore the pumping currents are negligible, as can be seen. With respect to the y direction, the system is finite and, furthermore, for GNRs with zigzag edges there is no strict reflection symmetry along this direction, see Fig. 2(a). For this reason, deviations from our previous reasoning are expected, and this explains that some current (although orders of magnitude smaller) can be appreciated for odd n_y. GNRs with armchair edges, on the other hand, do present a reflection symmetry along the y axis, see Fig. 2(b), so it is expected that the pumping currents are exactly zero for odd n_y.

We verified that the same type of behavior shown in Figs. 1(c) and 1(d) is also repeated for different Fermi energies and other sizes of the GNR, as long as the ribbon is not too small. Another general characteristic of the studied system is that the lower frequency modes yield, by far, the largest contribution to the pumping current. In particular, the mode that generates the highest value of $\tilde{I}_k$ is the one with $n_x = 1$ and $n_y = 0$. This is reasonable since, for this mode, the movement of all the sites contributes with the same sign to the pumping current and, thus, there are no cancellations. In Fig. 1(a), we depict the shape of this mode, while in Fig. 1(b) we show some other modes with negligible contributions to $\tilde{I}_k$. Based on the previous results, from now on we will only work with the mode with $n_x = 1$ and $n_y = 0$, denoting the scaled emissivity as $\tilde{I}_{(1,0)}$.

B. Fermi energy dependence

In this section, we will study how the maximum pumping current behaves for different values of the Fermi energy, ε_F. Again, we will consider both edges for the GNR. In Fig. 3, we show $\tilde{I}_{(1,0)}$ as a function of the Fermi energy for square nanoribbons of sides $L_x = L_y = 449\,a$ and for the mode with $n_x = 1$ and $n_y = 0$. In this figure, it can be seen that for large Fermi energies the type of edge does not seem to have an effect on the maximum value of the pumping current. In both cases, the pumping current increases roughly linearly with the number of conduction channels, which increases with the energy. For small Fermi energies, however, there is a clear difference in the behavior of the curves. In the case of aGNRs,

$\tilde{I}_{(1,0)}$ converges to a fixed value as ε_F goes to zero. Let us recall that because of the values of L_y used, there is always one conduction channel at $\varepsilon_F \approx 0$ for this type of nanoribbon. On the other hand, for zGNRs, the maximum value of the current increases rapidly as ε_F approaches zero. In fact, for $\varepsilon_F = 0$, the pumping current diverges, causing numerical problems in our calculations. This effect can be explained by noticing that zGNRs possess edge states at this energy with zero group velocity [30], causing the divergence of the associated density of states. The relation between the density of states and the pumped currents have been established in many different contexts [13,39].

To confirm that edge states are causing the abrupt increase of the pumping currents, we evaluate the contribution of each row of atoms to the total current by means of Eq. (24). In Fig. 2, it can be seen how these rows are defined for each nanoribbon type (see the green area). Figure 4 shows the contribution per row to $\tilde{I}_{(1,0)}$ for $\varepsilon_F = 0.001$ eV. As can be seen, zGNR rows close to the edges (located at $y = 0$ and $y = 449$) are the ones that contribute the most to $\tilde{I}_{(1,0)}$. On the contrary, aGNR rows near the edges do not seem to play any particular role in the currents. It should be mentioned that, in real systems, a true divergence of the pumping current is not expected since the coupling with the environment (causing, for example, decoherence [40]) should regularize it. However, at least a sharp peak of the pumping current should appear in potential experiments for $\varepsilon_F = 0$. In our case, without a specific model for the interaction with the environment, we cannot estimate the value of the pumping current precisely at this value. Finally, it is interesting to discuss the effect of finite temperatures in Fig. 3. Since the result of this is the convolution of the emissivity with the derivative of the Fermi-Dirac function [compare Eqs. (9) and (10)], its expected effect is simply to smooth (or average) the curves over a range of the order $k_B T$.[2]

According to the above discussion, there are two ways of increasing the pumped currents for zGNRs: either by adjusting the Fermi energy close to zero (and thus taking advantage of edge states and the divergence of the density of states that they cause) or by setting the Fermi energy to a large value (which naturally includes more conduction channels through which the current can be pumped). For aGNRs, the only available strategy is the second one.

C. Size dependence

In experiments with GNRs, these systems can sometimes have sizes on the order of a micrometer [41–44]. Since this involves a large number of atoms, performing numerical calculations for systems with those sizes involves an enormous computational cost. One way of estimating the value of the current $\tilde{I}_k$ for long nanoribbons is to study the behavior of this quantity as a function of size to make an extrapolation.

---

[2]Take into account that for Fermi energies ε_F too close to the Dirac point ($|\varepsilon_F| \lesssim k_B T$), the calculation of pumping currents at finite temperatures would present numerical issues due to the divergence of emissivities there, see Eq. (9).

We calculate the maximum value of the pumping current for square nanoribbons of different sizes $L = L_x = L_y$ and for both types of edges. The particular widths used (L_y values) were chosen such as to guaranty that the aGNRs are metallic. Based on the previous analysis, we took $n_x = 1$ and $n_y = 0$, and chose $\varepsilon_F = 0.1$ eV for the calculations. This value of ε_F is far enough from the Dirac point (thus avoiding numerical problems) and is, in principle, experimentally accessible [45].

In Fig. 5 we see, for both edges, that the log-log plot of $|\tilde{I}_k|$ with the size of the nanoribbons follows an approximate linear behavior for large values of L. There is also some dispersion around this linear behavior. However, this is not surprising since we are using the zero temperature limit of $\tilde{I}_k$, which is very sensitive to the density of states at the Fermi energy. Therefore, every time a new conduction channel appears at this energy (a consequence of an increase in L), a jump in the density of states is expected (due to the emergence of van Hove singularities), also causing a jump in $\tilde{I}_k$. The fittings shows that both edges follow an approximate quadratic dependence with L, for both edges. That is, the pumping currents scale with the surface of the system (L^2) and not with the width (L), as is the case of the zero-order current $I^{(0)}$ (proportional to the number of conduction channels at the studied energy).

According to the above results, we can estimate the value of $\tilde{I}_k$ for a square nanoribbon with sides close to one micrometer, $L \approx 4065\,a$. This gives an extrapolated scaled emissivity of approximately $\tilde{I}_k \sim 4 \times 10^4$ eV^{-1}. This value will be useful in the following section.

D. Realistic estimation of pumping currents

With the information collected so far, we are able to estimate the maximum value of the pumping current, $I^{(1)}_{L,(1,0),\max}$, in a realistic context. Just for the sake of comparison, we will take the amplitude factor as given by temperature only, see Eq. (22).

For the reasons discussed in the previous sections, we choose $n_x = 1$, $n_y = 0$, $\varepsilon_F = 0.1$ eV, and $L \approx 4065\,a$. With these parameters, the extrapolated value of the scaled emissivity in the low-temperature limit yields between 4.03×10^5 eV^{-1} (extrapolating for aGNRs) and 3.74×10^4 eV^{-1} (extrapolating for zGNRs). According to Eq. (22), we see that we still need to specify d_0, T, V_g, and A_{site} to obtain a concrete value for the current. The factor A_{site} is simply the area of the graphene unit cell divided by two, $A_{\text{site}} = 0.026$ nm^2. For the rest of the parameters, we took Ref. [41] as a guide, fixing the rest of the quantities at: $d_0 = 150$ nm, $T = 5$ K, and $V_g = 1$ V.

By substituting all the above values in Eq. (22), we obtain a value of $I^{(1)}_{L,(1,0),\max}$ between 1 and 10 pA. These contributions can be increased by taking advantage of the dependence of $I^{(1)}_{L,(1,0),\max}$ on d_0. For example, reducing the separation to $d_0 = 15$ nm, it follows that $I^{(1)}_{L,(1,0),\max}$ lies between 0.1 and 1 nA.

Just to put into context the above values of pumping currents, we can compare them with some measured values of currents in nanodevices. In Ref. [25], a fluctuation-induced current of the order of 10 pA is observed working with micrometric sheets of suspended graphene at temperatures two orders of magnitude higher than that used in our estimate. Another example is that of irradiated graphene experiments such as the one in Ref. [46], in which electric currents of the order of 10 pA at room temperature have also been measured. Working with mechanical resonators based on monolayer graphene, the authors of Ref. [6] measured currents of the order of pA at temperatures of 5 K. In conclusion, the estimated values of pumping currents induced by thermal vibrations seem plausible of being measured and, in principle, their effect should not be neglected since they can potentially interfere in some experiments.

Before continuing, here a comment is in order. The formalism used to describe the pumping current assumes that the vibrational degree of freedom behaves classically. This is valid as long as the vibrational energy is far from the zero point energy, which for thermal excitation implies $\hbar\omega_k/2k_B \ll T$. Considering a GNR with $L_x \sim 10^{-6}$ m, $n_x = 1$, $n_y = 0$, and taking $v \approx 12.9$ km/s [47], we estimate $\hbar\omega_{(1,0)}/2k_B \sim 0.05$ K. This very small temperature value also shows that the application of the equipartition theorem for the mechanical degrees of freedom used in Sec. II B does not contradict the low-temperature limit for the energy dependence of the electronic scattering matrix used in Eq. (10).

Finally, it is important to highlight that the presented estimations correspond to pumping currents induced by thermal excitations of the vibrational modes. Other forms of ambient vibrations, such as sound waves traversing the sample, could give rise to considerably larger amplitudes of the normal modes [increasing the amplitude factor in Eq. (22)] and thus much larger values of $I^{(1)}_{L,(1,0),\max}$ are possible. Therefore, the above estimations are the minimal expected values of the pumping currents in a real case scenario.

IV. CURRENT NOISE INDUCED BY THERMAL OSCILLATIONS OF GNRs

In previous sections, we show that fluctuation-induced pumping currents can be strong enough to be measurable, even for thermal excitations of the nanoribbons, affecting the observed currents of different nanodevices. Considering that stochastic fluctuations of the nanoribbons should induce what is essentially noise in the current determinations, it is fair to wonder how strong is this new form of noise, which we dubbed current noise induced by thermal vibrations (CNITV), as compared with more standard forms of current noise.

In this section, we develop a semiclassical approach to evaluate CNITV. This form of current noise is associated with the first-order terms of the adiabatic expansion of the current $\hat{I}^{(1)}$ (or pumping current) and should not be confused with Nyquist-Johnson or shot noise, which are due to zero-order terms of the current operator $\hat{I}^{(0)}$. In particular, we are wondering what the correlation function of the pumping currents is between contacts α and β, $S^{(1)}_{\alpha\beta}(\tau)$, induced by stochastic thermal variations of the parameters of a system's Hamiltonian. Here, we evaluate this quantity by means of

$$S^{(1,\text{sc})}_{\alpha\beta}(\tau) = \left\langle \left\{ \Delta I^{(1)}_\alpha(t) \Delta I^{(1)}_\beta(t') \right\}_s \right\rangle_c, \qquad (28)$$

where $\tau = t - t'$, $\{A_\alpha A_\beta\}_s = (A_\alpha A_\beta + A_\beta A_\alpha)/2$, $\langle...\rangle_c$ stands for the average over stochastic trajectories of the classical

parameters of the Hamiltonian,[3] and $\Delta I_\alpha^{(1)} = I_\alpha^{(1)} - \langle I_\alpha^{(1)}\rangle_c$. The pumping current $I_\alpha^{(1)}$ is the quantum expectation value $\langle ... \rangle$ of the first order current operator $\hat{I}_\alpha^{(1)}$, i.e., $I_\alpha^{(1)} = \langle \hat{I}_\alpha^{(1)}\rangle$. This expectation value is zero once averaged over stochastic trajectories, i.e., $\langle I_\alpha^{(1)}\rangle_c = \langle\langle \hat{I}_\alpha^{(1)}\rangle\rangle_c = 0$. Therefore, $\Delta I_\alpha^{(1)}$ is simply $I_\alpha^{(1)}$.

Note that Eq. (28) corresponds to a semiclassical approximation of the fully quantum current-noise [48,49]

$$S_{\alpha\beta}^{(1)}(\tau) = \langle\langle \{\Delta \hat{I}_\alpha^{(1)}(t)\Delta \hat{I}_\beta^{(1)}(t')\}_s\rangle\rangle_c, \quad (29)$$

where we replaced the current operators by their quantum expectation values. In this sense, at least for $\alpha = \beta$, Eq. (28) can be thought of as a lower limit to $S^{(1)}(\tau)$. First, note that their difference $\Delta S = S_{\alpha\alpha}^{(1)}(\tau) - S_{\alpha\alpha}^{(1,sc)}(\tau)$ gives

$$\Delta S = \{\langle\langle \hat{I}_\alpha^{(1)}(t)\hat{I}_\alpha^{(1)}(t')\rangle\rangle_c - \langle\langle \hat{I}_\alpha^{(1)}(t)\rangle\langle \hat{I}_\alpha^{(1)}(t')\rangle\rangle_c\}_s. \quad (30)$$

Now, for $\tau = 0$, it holds

$$\langle[\hat{I}_\alpha^{(1)}(t)]^2\rangle - \langle\hat{I}_\alpha^{(1)}(t)\rangle^2 \geqslant 0, \quad (31)$$

due to the Cauchy–Schwarz inequality, while for $\tau \to \infty$,

$$\langle\langle \hat{I}_\alpha^{(1)}(t)\hat{I}_\alpha^{(1)}(t')\rangle\rangle_c = \langle\langle \hat{I}_\alpha^{(1)}(t)\rangle\rangle_c = 0, \quad (32)$$

since each trajectory of the classical parameters over which we are averaging is stochastic. Therefore, $S_{\alpha\alpha}^{(1)} \geqslant S_{\alpha\alpha}^{(1,sc)}$ for $\tau = 0$ and $S_{\alpha\alpha}^{(1)} = S_{\alpha\alpha}^{(1,sc)} = 0$ for $\tau \to \infty$. In our case, the time-dependent variation of the acoustic transversal modes of graphene $q_i(t)$ is the origin of the current noise, and thus

$$\Delta I_\alpha^{(1)}(t) = e \sum_k \left(\frac{dn_\alpha}{dq_k}\right)(\dot{q}_k(t) - \langle\dot{q}_k(t)\rangle_c). \quad (33)$$

Replacing this in Eq. (28), taking into account that velocities of different modes are not correlated, i.e., $\langle\dot{q}_k\dot{q}_{k'}\rangle_c = \langle\dot{q}_k\rangle_c\langle\dot{q}_{k'}\rangle_c$, and that their stochastic average is zero, $\langle\dot{q}_k(t)\rangle_c = 0$, we obtain

$$S_{\alpha\beta}^{(1,sc)}(\tau) = e^2 \sum_k \left(\frac{dn_\alpha}{dq_k}\right)\left(\frac{dn_\beta}{dq_k}\right)\langle\dot{q}_k(t)\dot{q}_k(t')\rangle_c. \quad (34)$$

Now we will assume a generic model for the autocorrelation function of velocities

$$\langle\dot{q}_k(t)\dot{q}_k(t')\rangle_c \approx \frac{k_B T}{m_c}e^{-|t-t'|/\tau_k}, \quad (35)$$

which fulfills the equipartition theorem for $t = t'$, while including the effects of a finite correlation time τ_k for each normal mode k. This kind of exponentially decaying correlation function can indeed be derived analytically for simple

models; see, for example, Ref. [50]. Inserting Eq. (35) into Eq. (34) and taking the limit of small τ_k gives[4]

$$S_{\alpha\beta}^{(1,sc)}(\tau) \approx \left[\frac{2e^2 k_B T}{m_c} \sum_k \left(\frac{dn_\alpha}{dq_k}\right)\left(\frac{dn_\beta}{dq_k}\right)\tau_k\right]\delta(\tau), \quad (36)$$

where the term in brackets is the zero-frequency noise of the CNITV, $S_{\alpha\beta}^{(1,sc)}(\omega = 0)$. It is interesting to compare this term with the Nyquist-Johnson zero-frequency noise, $S_{\alpha\beta}^{(NJ)}(\omega = 0)$, typically used to assess current noise. In the limit of small temperature, the latter is given as [51]

$$S_{\alpha\beta}^{(NJ)}(\omega = 0) = -4k_B T \frac{e^2}{h} \sum_{\eta \in \alpha, \eta' \in \beta} T_{\eta\eta'}, \quad (37)$$

where $T_{\eta\eta'}$ is the transmission coefficient between conduction channels η and η' belonging to contacts α and β, respectively, and $T_{\eta\eta} = -\sum_{\eta \neq \eta'} T_{\eta\eta'}$. If we wonder when $S_{\alpha\alpha}^{(1,sc)}(\omega = 0)$ will be the dominant source of current noise, i.e., $S_{\alpha\alpha}^{(1,sc)} > S_{\alpha\alpha}^{(NJ)}$, this implies the condition, in the low temperature limit,

$$\frac{h}{2m_c}\left(\frac{\partial E}{\partial z}\right)^2 \tilde{I}_{(1,0)}^2 \tau_{(1,0)} \gtrsim -\sum_{\eta, \eta' \in \alpha} T_{\eta\eta'}, \quad (38)$$

where the right-hand side of the equation is the total transmittance and, in agreement with the previous sections, we assume that the mode $(n_x, n_y) = (1, 0)$ gives the dominant contribution to the pumped current.

Typically, defects in quasi-one-dimensional systems like GNRs reduce dramatically the transmittance while pumping currents are not necessarily affected in the same way. Indeed, the peaks in the density of states caused by defects can favorably affect the pumping currents [13]. The scaling with the length of the sample also favors pumping currents. Note that the emissivity is approximately proportional to the length of the system [as Eq. (24) suggests], while the total transmittance in the coherent limit of the current is, at best, independent of the length of the sample. Let us recall that, in quasi-one-dimensional systems with defects, the transmittance is exponentially suppressed with the length [52,53].

The above reasoning sets some general conditions where one would expect the CNITV to be the dominant contribution to the current noise: elongated samples with defects. For example, we consider a GNR with $L_x = 800\,a$, $L_y = 200\,a$ (which gives $\omega_{(1,0)} = 1.9 \times 10^{11}$ rad/s), 0.5% of vacancies randomly distributed, $\varepsilon_F = 0.1$ eV, $d_0 = 15$ nm, and $V_g = 1$ V. With these parameters, we obtained, after 70 independent runs giving different pairs of scaled emissivities and transmittances, that in 83% of the samples $\tau_{(1,0)} = 1.05 \times 10^{-8}$ s is enough to make the CNITV the dominant contribution to current noise. This means that a quality factor (taking $Q = \tau_k\omega_k/2$) of only 10^3 is required, which is a modest value compared with what is possible experimentally for graphene

---

[3]The electronic Hamiltonian H varies when the GNR oscillates with a given normal mode (as explained in Sec. II D). Let us recall that the movement of the GNR is considered classically here, so q (the vector containing the amplitude of the normal modes) is a parameter of H. In our paper, we are considering small amplitudes of the normal modes, so $q(t) \approx q_0$. However, $\dot{q}$ will still change stochastically due to thermal fluctuations. Therefore, when calculating the current noise, one has to average over the stochastic variation of $\dot{q}$, that is, $\langle ... \rangle_c$, which is different from $\langle ... \rangle$, the expectation value of some quantity.

---

[4]This limit means that correlations decay instantaneously as compared with the measurement time. This would lead $S(\tau)$ to be proportional to the Dirac delta function (with a proportionality factor equal to the so called zero-frequency noise), which is an usual assumption in noise treatment.

resonators at low temperatures [54]. Increasing vacancies up to 1% makes that a quality factor of 10^3 suffices for 92% of the samples.

V. CONCLUSIONS

Motivated by the implementation of GNRs as pumps, sensors, and recent experiments on thermal fluctuation-induced currents, here we developed a theoretical and numerical model to study the instantaneous value of quantum pumping currents in these systems. In particular, we focused on calculating the maximum value of the pumping current that arises from the excitation of the transverse acoustic modes of suspended GNRs. Although our calculations are strictly valid under certain conditions (namely, classical limit of vibrations, small oscillations, low frequency transversal acoustic modes, large ribbon sizes, and the low-temperature limit), our results can be helpful in estimating the magnitude of this type of current. In this context, the developed theoretical tools and our results allow one to understand the role of the different parameters in the fluctuation-induced currents and assess under which conditions these currents can play an important role in actual experiments.

As particular results of the geometry studied, we found that pumping currents increase with the size of the system, being approximately proportional to the area of the ribbon and independent of the edge geometry for large sizes. The lowest frequency modes contribute the most to the pumping currents. The contribution of modes with n_x even or n_y odd is negligible, being strictly zero when the size of the system tends to infinity. While for large Fermi energies there are no significant differences between zigzag and armchair GNRs, for energies close to the Dirac point marked divergences appear. The behavior of aGNRs depends on their width, which makes them metallic or semiconductor. Metallic aGNRs present a relatively small and energy-independent pumping current, while semiconductor aGNRs have zero pumping current for Fermi energy close to the Dirac point. On the contrary, zGNRs present a strong increase of pumping currents close to the Dirac point due to the presence of their edge states.

Our estimations of GNRs' pumping currents in the studied geometries indicate that, in principle, even thermal fluctuations of the ribbons should produce measurable currents and that their effects should not be negligible for several experimental setups. It is worth noting that other forms of excitation of the GNRs, such as propagating sound waves traversing the system, are potentially even more favorable for inducing pumping currents.

Finally, we developed a semiclassical theory to evaluate the CNITV. The comparison with Nyquist-Johnson noise allowed us to set some general conditions where one would expect the CNITV to be the dominant contribution to the current noise: elongated samples with defects.

Our results, which include quantum effects, could provide a more accurate calculation of fluctuation-induced currents in experiments like the one in Ref. [25]. Given that sensing is ultimately limited by the signal-to-noise ratio, our results can also help to improve the design of sensors based on suspended GNRs. This could be done, e.g., in optimal configurations that minimize current noise and/or maximize the signal of the fluctuation-induced current coming from a specific oscillation of the ribbon. If fluctuating currents arising from the oscillation of GNRs could be rectified (which would depend on the frequency and the magnitude of the current), then our results could be used to design energy harvesters that turn ambient mechanical excitations (above the thermal level) into electric power.

There are several further aspects that could be studied, including other vibrational modes, and different systems like carbon nanotubes or heterogeneous multilayer 2D materials. To assess the role of anharmonicities in the pumping currents, large oscillation amplitudes of the modes can be explored. Also, the effect of finite bias voltages on the induced current, or even the consequences of local voltage thermal fluctuations, give rise to interesting directions to follow. In this regard, the present paper paves the way to explore these and other exciting directions.

APPENDIX A: TRANSVERSE NORMAL MODES OF A RECTANGULAR ELASTIC MEMBRANE

As mentioned in Sec. II B, to study the vibrations in a GNR we will consider that the suspended system is large enough to be approximated by a rectangular elastic membrane. Assuming that the equilibrium position of the membrane defines the xy plane, we will call $z(x, y, t)$ the displacement of the membrane with respect to said plane. This variable z satisfies the wave equation

$$\nabla^2 z = \frac{1}{v^2}\frac{\partial^2 z}{\partial t^2}, \qquad (A1)$$

where v is the speed of propagation of the wave. Making the replacement $z = F(x, y)q(t)$, we separate the above equation into a spatial equation (Helmholtz equation) and a temporal equation:

$$(\nabla^2 + k^2)F = 0, \quad \ddot{q} + k^2 v^2 q = 0. \qquad (A2)$$

The solutions to the temporal equation are of the form

$$q(t) = A\cos(kvt) + B\sin(kvt), \qquad (A3)$$

while for the spatial part it is necessary to specify the boundary conditions. Once the corresponding eigenfunctions have been obtained, the general time-dependent solution, $z(x, y, t)$, can be constructed by superposition. Going back to the Helmholtz equation, it has the form

$$\frac{\partial^2 F}{\partial x^2} + \frac{\partial^2 F}{\partial y^2} + k^2 F = 0. \qquad (A4)$$

If the boundary conditions are separated in the x and y directions, we can apply separation of variables in the form $F(x, y) = X(x)Y(y)$. Substituting this into Eq. (A4) and dividing by F gives

$$k^2 + \frac{1}{X}\frac{dX^2}{dx^2} = -\frac{1}{Y}\frac{dY^2}{dy^2}. \tag{A5}$$

The left hand side is a function of x only, while the right hand side is a function of y only. Therefore, this relation is only valid if both sides are equal to a constant. With this in mind, we write

$$\frac{dX^2}{dx^2} = -k_x^2 X, \tag{A6}$$

and

$$\frac{dY^2}{dy^2} = -k_y^2 Y, \tag{A7}$$

with k_x and k_y satisfying the relation $k_x^2 + k_y^2 = k^2$. Thus, the two-dimensional problem has been reduced to two one-dimensional problems, whose solutions are

$$X(x) = C_x \cos(k_x x) + D_x \sin(k_x x),$$
$$Y(y) = C_y \cos(k_y y) + D_y \sin(k_y y). \tag{A8}$$

We are now in position to specify the boundary conditions of the problem. We will think of a rectangular membrane with side L_x on the x axis and side L_y on the y axis, with the two edges in the x direction fixed and the two edges in the y direction free. This implies that the separate solutions of Eqs. (A6) and (A7) must comply with $X(0) = X(L_x) = 0$ and $Y'(0) = Y'(L_y) = 0$ to ensure that the membrane does not move at the fixed edges and that there is zero slope at the free edges. Applying these conditions, we arrive at

$$C_x = 0, \quad k_x = \frac{n_x \pi}{L_x}, \quad n_x = 0, 1, 2, \dots \tag{A9}$$

and

$$D_y = 0, \quad k_y = \frac{n_y \pi}{L_y}, \quad n_y = 0, 1, 2, \dots, \tag{A10}$$

and, in consequence:

$$X(x) = \sin(k_x x), \quad Y(y) = \cos(k_y y). \tag{A11}$$

In conclusion, the solution of the spatial problem is of the form

$$F_{n_x, n_y}(x, y) = \sin\left(\frac{n_x \pi}{L_x}x\right)\cos\left(\frac{n_y \pi}{L_y}y\right), \tag{A12}$$

with

$$k_{n_x, n_y}^2 = \frac{\omega_{n_x, n_y}^2}{v^2} = \left(\frac{n_x \pi}{L_x}\right)^2 + \left(\frac{n_y \pi}{L_y}\right)^2. \tag{A13}$$

The general solution to the two-dimensional wave equation can then be obtained by superposition of the normal modes, resulting, in this case, in Eq. (2) of the main text:

$$z(x, y, t) = \sum_{n_x=0}^{\infty}\sum_{n_y=0}^{\infty}\sin\left(\frac{n_x \pi}{L_x}x\right)\cos\left(\frac{n_y \pi}{L_y}y\right)q(t). \tag{A14}$$

APPENDIX B: ENERGY OF NORMAL MODES

The total energy of a system composed of atoms labeled by i, and considering only the z component of their respective positions for simplicity, is

$$E_{\text{tot}} = \sum_i m_i \frac{\dot{z}_i^2}{2} + U_{\text{tot}}(z), \tag{B1}$$

where m_i is the mass of the atom i and U_{tot} is the total potential energy of the system. As usual, in any harmonic approximation we expand the potential up to second order in the displacement around the equilibrium position z_0 (here sets equal to zero for simplicity). Using this, we obtain

$$E_{\text{tot}} - U_{\text{tot}}(z_0) \approx \frac{m_c}{2}\left(\dot{z}^{\mathrm{T}}\dot{z} + \frac{1}{m_c}z^{\mathrm{T}}\mathcal{H}z\right), \tag{B2}$$

where $\mathcal{H}$ is the Hessian matrix. Now, assuming all masses are equal ($m_i = m_c$) and inserting $U^{\mathrm{T}}U = I$, where $U\mathcal{H}U^T/m_c = \Omega_q$ with Ω_q the diagonal matrix containing the square frequency of normal modes, the energy results in

$$E_{\text{tot}} - U_{\text{tot}}(z_0) \approx \frac{m_c}{2}(\dot{z}^{\mathrm{T}}U^{\mathrm{T}}U\dot{z} + z^{\mathrm{T}}U^{\mathrm{T}}\Omega_q Uz). \tag{B3}$$

Finally, we recognize $q = Uz$ as the coordinate vector of the normal modes [which, in our case, we approximate as the q_k of Eq. (2)]. Then, the energy can be written as

$$E_{\text{tot}} - U_{\text{tot}}(z_0) \approx \frac{m_c}{2}(\dot{q}^{\mathrm{T}}\dot{q} + q^{\mathrm{T}}\Omega_q q) = \sum_k E_k, \tag{B4}$$

with $E_k = m_c(\dot{q}_k^2 + \omega_k^2 q_k^2)/2$ being the energy of the normal mode k.

APPENDIX C: VALIDITY OF THE ADIABATIC APPROXIMATION

Adiabatic quantum pumping arises from the first-order correction (in a frequency expansion) to the adiabatic approximation of an observable, the current in our case. Technical details of its derivation can be found among different contexts [27,35,39,55,56]. In the present case, the adiabatic approximation and its first-order correction will be valid when the time it takes for the electrons to move along the lattice sites is much shorter than the time it takes for the Hamiltonian to change. To assess this, we take a mode with some value n_x of a GNR of length L_x ($n_y = 0$ for simplicity). The time τ_e electrons take to move (in a fluctuating GNR) between regions with the maximum and minimum values of the on-site energies is $\tau_e = L_x/(2n_x v_F)$, where v_F is the Fermi velocity. The frequency of the normal modes is given by Eq. (4), which sets the variation frequency of the electronic Hamiltonian. Taking $v_F = 10^6$ m/s and $v_T = 12.9 \times 10^3$ m/s (the velocity of sound for GNR transversal modes) yields a ratio between τ_e and the period of the vibration $\tau_{\text{mech}} = 2\pi/\omega_{n_x, n_y}$ of 3.23×10^{-3}, which is a reasonably small value for the expansion. Remarkably, for $n_y = 0$ this ratio is independent of the vibrational mode n_x and, given the expression for $\tau_e/\tau_{\text{mech}}$, we do not expect large variations from this ratio for small values of n_y.

APPENDIX D: PARALLEL PLATE MODEL

The goal of this Appendix is to give an expression for the factor $\partial_z E$. The key idea is using the principle of correspondence between the quantum system described in Sec. II A and its classical analog taken as the capacitor formed by a continuous conductive membrane (the GNR) separated by a distance d_0 from the gate with a potential difference V_g. To simplify the derivation, we will assume that the GNR can only move as a whole in the z direction, such that the classical analog is simply a parallel plate capacitor with separation d_0 between the plates. In this way, z_i will be the same for all sites and the change in the on-site energies will also be the same, i.e., $\partial_z \boldsymbol{H}^{(E)} = (\partial_z E)\boldsymbol{I}$, with $\boldsymbol{I}$ the identity matrix. To simplify the notation, from now on we will omit the superscript (E) since we will be always working with the part of the Hamiltonian that represents the variations in the site energies of the system. Now, the question that we want to answer is the following: What is the value of $\partial_z E$ in the tight-binding Hamiltonian such that the system behaves as a parallel plate capacitor in the limit of large membranes?

Consider the energy of a capacitor with parallel plates of area A, a potential V_g, and separated by a distance d. The energy stored in this "classical" capacitor is

$$E^{(\text{classic})} = \frac{1}{2}CV_g^2 = \frac{\epsilon_0 A}{2d}V_g^2. \tag{D1}$$

If we now think of small z displacements from a given equilibrium position d_0, we can approximate the new energy as

$$\begin{aligned} E^{(\text{classic})} &\approx E_0^{(\text{classic})} + \left.\frac{\partial E^{(\text{classic})}}{\partial z}\right|_{d_0} z \\ &= E_0^{(\text{classic})} + \left(-\frac{\epsilon_0 A}{2d_0^2}V_g^2\right)z. \end{aligned} \tag{D2}$$

Now considering the Hamiltonian model of the system, the total energy (near equilibrium) is

$$\begin{aligned} \langle \hat{H} \rangle &= \text{Tr}[\hat{H}\hat{\rho}^{(\text{eq})}] \\ &\approx \langle \hat{H}_0 \rangle + \text{Tr}[(\partial_z \hat{H})\hat{\rho}^{(\text{eq})}]z + \text{Tr}[\hat{H}\partial_z\hat{\rho}^{(\text{eq})}]z \\ &\approx \langle \hat{H}_0 \rangle + \left(\sum_i (\partial_z H_{ii})\rho_{ii}^{(\text{eq})}\right)z \\ &\quad + \left(\sum_{ij} H_{ij}\partial_z\rho_{ji}^{(\text{eq})}\right)z, \end{aligned} \tag{D3}$$

where we perform an expansion in z around the equilibrium position z_0. Here $\langle \hat{H}_0 \rangle$ is the average energy of the system at equilibrium ($z=0$). Note that $\hat{\rho}^{(\text{eq})}$ is diagonal in the energy basis, but not necessarily in the i position basis.

To find $\partial_z E$, we are going to demand that, in the limit of large systems, the change in the total energy of the system corresponds to that expected for the parallel plate capacitor described above. This implies working Eq. (D3) and then performing a comparison with Eq. (D1) in the limit of macroscopic systems.

First, starting from Eq. (D3), we will show that the term with $\partial_z\rho_{ji}^{(\text{eq})}$ is zero. To easily calculate this amount, we are

going to assume that

$$\hat{\rho}_{\text{tot}}^{(\text{eq})} = \hat{\rho}_{\text{leads}}^{(\text{eq})} \otimes \hat{\rho}_{\text{sys}}^{(\text{eq})}, \quad \hat{\rho}_{\text{sys}}^{(\text{eq})} = \frac{\exp[-\beta(\hat{H}_{\text{sys}} - \mu\hat{N})]}{\Phi_{\text{sys}}}, \tag{D4}$$

where $\Phi_{\text{sys}} = \text{Tr}[\exp(-\beta(\hat{H} - \mu\hat{N}))]$ and $\beta = 1/k_\text{B}T$. Then, taking the Hamiltonian of the system [see Eq. (12)] and setting $H_{\text{sys}} \equiv H$, we see that its derivatives are of the form

$$\partial_z\hat{H} = \left(\frac{\partial E}{\partial z}\right)\hat{1} \quad \Rightarrow \quad \partial_z\hat{H}^n = n\left(\frac{\partial E}{\partial z}\right)\hat{H}^{n-1}. \tag{D5}$$

Similarly, it holds

$$\partial_z(\hat{H} - \mu\hat{N}) = \left(\frac{\partial E}{\partial z}\right)\hat{1}, \tag{D6}$$

and then

$$\partial_z(\hat{H} - \hat{N})^n = n\left(\frac{\partial E}{\partial z}\right)(\hat{H} - \mu\hat{N})^{n-1}. \tag{D7}$$

Using these results, it is possible to calculate the derivative of the equilibrium density matrix

$$\partial_z\rho_{ji}^{(\text{eq})} = \langle j|\frac{\partial_z e^{-\beta(\hat{H}-\mu\hat{N})}}{\Phi}|i\rangle + \langle j|e^{-\beta(\hat{H}-\mu\hat{N})}\partial_z\left(\frac{1}{\Phi}\right)|i\rangle. \tag{D8}$$

Working with the first term, we get

$$\langle j|\partial_z\left(\frac{e^{-\beta(\hat{H}-\mu\hat{N})}}{\Phi}\right)|i\rangle = (-\beta)\left(\frac{\partial E}{\partial z}\right)\rho_{ji}^{(\text{eq})}. \tag{D9}$$

On the other hand, working the second term, we arrive at

$$\langle j|e^{-\beta(\hat{H}-\mu\hat{N})}\partial_z\left(\frac{1}{\Phi}\right)|i\rangle = \beta\left(\frac{\partial E}{\partial z}\right)\rho_{ji}^{(\text{eq})}. \tag{D10}$$

Thus, joining the two previous results yields $\partial_z\rho_{ji}^{(\text{eq})} = 0$.

The fact that $\partial_z\rho_{ji}^{(\text{eq})} = 0$ and the assumption $\partial_z H = (\partial E/\partial z)\boldsymbol{I}$ allows us to write $\langle H \rangle$ as

$$\langle H \rangle \approx \langle H_0 \rangle + \left(\frac{\partial E}{\partial z}\right)n_{\text{sys}}^{(\text{eq})}z, \tag{D11}$$

where $n_{\text{sys}}^{(\text{eq})} = (\sum_i \rho_{ii}^{(\text{eq})})$ is the mean number of particles within the system at equilibrium. Therefore, for our Hamiltonian model to be consistent with macroscopic theory, we must do

$$\lim_{A\to\infty}\left(-\frac{1}{2}\epsilon_0\frac{A}{d_0^2}V_g^2\right)z = \lim_{A\to\infty}\left(\frac{\partial E}{\partial z}\right)n_{\text{sys}}^{(\text{eq})}z, \tag{D12}$$

which gives

$$\left(\frac{\partial E}{\partial z}\right) = \frac{-\dfrac{1}{2}\dfrac{\epsilon_0 V_g^2}{d_0^2}}{\lim\limits_{A\to\infty}\dfrac{n_{\text{sys}}^{(\text{eq})}}{A}}. \tag{D13}$$

Note that $n_{\text{sys}}^{(\text{eq})}$ is the number of sites multiplied by 1/2 (since two electrons enter per site according to the Pauli exclusion principle), and that the total area A can be thought of as the

number of sites multiplied by the area occupied by each site, A_{site}. Then we can write

$$\lim_{A \to \infty} \frac{n_{\text{sys}}^{(\text{eq})}}{A} = \frac{1}{2A_{\text{site}}} \tag{D14}$$

and, in consequence,

$$\left(\frac{\partial E}{\partial z} \right) = -\epsilon_0 \frac{A_{\text{site}} V_g^2}{d_0^2}. \tag{D15}$$

APPENDIX E: PUMPING CURRENTS DUE TO COUPLING VARIATIONS

In this Appendix, we will show that, in the limit of small oscillations of flexural modes, the contribution to the pumping current due to hopping variations between neighboring atoms can be neglected. More specifically, this involves deriving Eq. (19) and proving that $\partial S^{(V)}/\partial q_k$ tends to zero in the perturbative limit. To carry out this task, we will use the matrix form of the Fisher-Lee formula [28,57,58]:

$$S = I - 2iW^\dagger G^R W. \tag{E1}$$

Here, G^R is the retarded Green's function given by

$$G^R = \lim_{\eta \to 0^+} [(\varepsilon + i\eta)I - H - \Sigma^R]^{-1}, \tag{E2}$$

where H is the Hamiltonian of the system without the contacts, Σ^R is the retarded self-energy due to the contacts, and ε is the energy of the electrons. The matrix W comes from the relation

$$\Gamma_\alpha = W^\dagger \Pi_\alpha W, \tag{E3}$$

where Π_α is the projection operator towards the channel α of some reservoir r, and Γ_α is the contribution, due to channel α, of the imaginary part of the self-energy Σ^R, i.e., $\Gamma = -\text{Im}(\Sigma^R)$ and $\Gamma = \sum_\alpha \Gamma_\alpha$.

Using Eq. (E1) and $\partial G^r = -G^r \partial [G^r]^{-1} G^r$, we find

$$\frac{\partial S}{\partial q_k} = (-2i)W^\dagger G^r \frac{\partial H^{(E)}}{\partial q_k} G^r W$$

$$+ (-2i)W^\dagger G^r \frac{\partial H^{(V)}}{\partial q_k} G^r W$$

$$= \frac{\partial S^{(E)}}{\partial q_k} + \frac{\partial S^{(V)}}{\partial q_k}, \tag{E4}$$

proving Eq. (19).

Now, using the chain rule

$$\frac{\partial H^{(V)}}{\partial q_k} = \sum_\ell \frac{\partial H^{(V)}}{\partial z_\ell} \frac{\partial z_\ell}{\partial q_k}, \tag{E5}$$

where z_ℓ is the displacement of atom ℓ in the z direction, and studying the matrix elements of $\partial H^{(V)}/\partial z_\ell$ when the system is in equilibrium, we arrive at

$$\left(\frac{\partial H_{ij}^{(V)}}{\partial z_\ell} \right)_{q_0} = \left[(z_i - z_j) \frac{t_0 b}{a_{\text{cc}}} \frac{\partial}{\partial z_\ell} (z_i - z_j) \right]_{q_0}. \tag{E6}$$

Since evaluating at q_0 implies taking $z_i = 0$, $\forall i$, we have that

$$\left(\frac{\partial H_{ij}^{(V)}}{\partial z_\ell} \right)_{q_0} \sim (z_i - z_j)_{q_0} = 0. \tag{E7}$$

In short, for small oscillations around the equilibrium position, the hopping variation does not contribute to the pumping current induced by flexural modes.

[1] C. Lee, X. Wei, J. W. Kysar, and J. Hone, Measurement of the elastic properties and intrinsic strength of monolayer graphene, Science **321**, 385 (2008).

[2] J.-H. Chen, C. Jang, S. Xiao, M. Ishigami, and M. S. Fuhrer, Intrinsic and extrinsic performance limits of graphene devices on SiO$_2$, Nat. Nanotechnol. **3**, 206 (2008).

[3] S. Chen, A. L. Moore, W. Cai, J. W. Suk, J. An, C. Mishra, C. Amos, C. W. Magnuson, J. Kang, L. Shi, and R. S. Ruoff, Raman measurements of thermal transport in suspended monolayer graphene of variable sizes in vacuum and gaseous environments, ACS Nano **5**, 321 (2011).

[4] J. S. Bunch, A. M. van der Zande, S. S. Verbridge, I. W. Frank, D. M. Tanenbaum, J. M. Parpia, H. G. Craighead, and P. L. McEuen, Electromechanical resonators from graphene sheets, Science **315**, 490 (2007).

[5] D. Garcia-Sanchez, A. M. van der Zande, A. S. Paulo, B. Lassagne, P. L. McEuen, and A. Bachtold, Imaging mechanical vibrations in suspended graphene sheets, Nano Lett. **8**, 1399 (2008).

[6] C. Chen, S. Rosenblatt, K. I. Bolotin, W. Kalb, P. Kim, I. Kymissis, H. L. Stormer, T. F. Heinz, and J. Hone, Performance of monolayer graphene nanomechanical resonators with electrical readout, Nat. Nanotechnol. **4**, 861 (2009).

[7] A. Croy, D. Midtvedt, A. Isacsson, and J. M. Kinaret, Nonlinear damping in graphene resonators, Phys. Rev. B **86**, 235435 (2012).

[8] R. Zhu and H. Chen, Quantum pumping with adiabatically modulated barriers in graphene, Appl. Phys. Lett. **95**, 122111 (2009).

[9] E. Prada, P. San-Jose, and H. Schomerus, Quantum pumping in graphene, Phys. Rev. B **80**, 245414 (2009).

[10] L. E. F. Foa Torres, H. L. Calvo, C. G. Rocha, and G. Cuniberti, Enhancing single-parameter quantum charge pumping in carbon-based devices, Appl. Phys. Lett. **99**, 092102 (2011).

[11] P. San-Jose, E. Prada, S. Kohler, and H. Schomerus, Single-parameter pumping in graphene, Phys. Rev. B **84**, 155408 (2011).

[12] T. Low, Y. Jiang, M. Katsnelson, and F. Guinea, Electron pumping in graphene mechanical resonators, Nano Lett. **12**, 850 (2012).

[13] L. H. Ingaramo and L. E. F. Foa Torres, Quantum charge pumping in graphene-based devices: When lattice defects do help, Appl. Phys. Lett. **103**, 123508 (2013).

[14] M. R. Connolly, K. L. Chiu, S. P. Giblin *et al.*, Gigahertz quantized charge pumping in graphene quantum dots, Nat. Nanotechnol. **8**, 417 (2013).

[15] X. Zang, Q. Zhou, J. Chang, Y. Liu, and L. Lin, Graphene and carbon nanotube (CNT) in MEMS/NEMS applications, Microelectron. Eng. **132**, 192 (2015).

[16] B. Davaji, H. Cho, M. Malakoutian, J.-K. Lee, G. Panin, T. Kang, and C. Lee, A patterned single layer graphene resistance temperature sensor. Sci. Rep. **7**, 8811 (2017).

[17] Z. H. Khan, A. R. Kermany, A. Öchsner, and F. Iacopi, Mechanical and electromechanical properties of graphene and their potential application in MEMS, J. Phys. D **50**, 053003 (2017).

[18] D. Moreno-Garcia, X. Fan, A. D. Smith, M. C. Lemme, V. Messina, C. Martin-Olmos, F. Niklaus, and L. G. Villanueva, A resonant graphene nems vibrometer, Small **18**, 2201816 (2022).

[19] R. K. Gupta, F. H. Alqahtani, O. M. Dawood, M. Carini, A. Criado, M. Prato, S. K. Garlapati, G. Jones, J. Sexton, K. C. Persaud, C. Dang, U. Monteverde, M. Missous, R. J. Young, S. Boult, N. Dixon, L. Majewski, and M. A. Migliorato, Suspended graphene arrays for gas sensing applications, 2D Mater. **8**, 025006 (2021).

[20] M. Liao and Y. Koide, Carbon-based materials: Growth, properties, MEMS/NEMS technologies, and MEMS/NEMS switches, Crit. Rev. Solid State Mater. Sci. **36**, 66 (2011).

[21] X. Fan, F. Forsberg, A. Smith, S. Schröder, S. Wagner, H. Rödjegård, A. Fischer, M. Östling, M. C. Lemme, and F. Niklaus, Graphene ribbons with suspended masses as transducers in ultra-small nanoelectromechanical accelerometers. Nat. Electron. **2**, 394 (2019).

[22] Y. Ben-Shimon, C. P. Sharma, C. J. Arnusch, and A. Ya'akobovitz, Freestanding laser-induced graphene ultrasensitive resonative viral sensors, ACS Appl. Mater. Interfaces **14**, 44713 (2022).

[23] J. B. Johnson, Thermal agitation of electricity in conductors, Phys. Rev. **32**, 97 (1928).

[24] H. Nyquist, Thermal agitation of electric charge in conductors, Phys. Rev. **32**, 110 (1928).

[25] P. M. Thibado, P. Kumar, S. Singh, M. Ruiz-Garcia, A. Lasanta, and L. L. Bonilla, Fluctuation-induced current from freestanding graphene, Phys. Rev. E **102**, 042101 (2020).

[26] P. W. Brouwer, Scattering approach to parametric pumping, Phys. Rev. B **58**, R10135(R) (1998).

[27] N. Bode, S. V. Kusminskiy, R. Egger, and F. von Oppen, Scattering theory of current-induced forces in mesoscopic systems, Phys. Rev. Lett. **107**, 036804 (2011).

[28] R. A. Bustos-Marún, Geometric rectification for nanoscale vibrational energy harvesting, Phys. Rev. B **97**, 075412 (2018).

[29] S. H. Kim, C. S. Haines, N. Li, K. J. Kim, T. J. Mun, C. Choi, J. Di, Y. J. Oh, J. P. Oviedo, J. Bykova, S. Fang, N. Jiang, Z. Liu, R. Wang, P. Kumar, R. Qiao, S. Priya, K. Cho, M. Kim, M. S. Lucas *et al.*, Harvesting electrical energy from carbon nanotube yarn twist, Science **357**, 773 (2017).

[30] L. Foa Torres, S. Roche, and J. Charlier, *Introduction to Graphene-Based Nanomaterials: From Electronic Structure to Quantum Transport* (Cambridge University Press, New York, 2020).

[31] A. Cresti, N. Nemec, B. Biel, G. Niebler, F. Triozon, G. Cuniberti, and S. Roche, Charge transport in disordered graphene-based low dimensional materials, Nano Res. **1**, 361 (2008).

[32] S. Dutta and S. K. Pati, Novel properties of graphene nanoribbons: A review, J. Mater. Chem. **20**, 8207 (2010).

[33] P. W. Anderson, Local moments and localized states, Rev. Mod. Phys. **50**, 191 (1978).

[34] J. Splettstoesser, M. Governale, J. König, and R. Fazio, Adiabatic pumping through interacting quantum dots, Phys. Rev. Lett. **95**, 246803 (2005).

[35] L. Arrachea and M. Moskalets, Relation between scattering-matrix and Keldysh formalisms for quantum transport driven by time-periodic fields, Phys. Rev. B **74**, 245322 (2006).

[36] H. Li, L. J. Fernández-Alcázar, F. Ellis, B. Shapiro, and T. Kottos, Adiabatic thermal radiation pumps for thermal photonics, Phys. Rev. Lett. **123**, 165901 (2019).

[37] V. M. Pereira, A. H. Castro Neto, and N. M. R. Peres, Tight-binding approach to uniaxial strain in graphene, Phys. Rev. B **80**, 045401 (2009).

[38] C. W. Groth, M. Wimmer, A. R. Akhmerov, and X. Waintal, Kwant: A software package for quantum transport, New J. Phys. **16**, 063065 (2014).

[39] S. E. Deghi, L. J. Fernández-Alcázar, H. M. Pastawski, and R. A. Bustos-Marún, Current-induced forces in single-resonance systems, J. Phys.: Condens. Matter **33**, 175303 (2021).

[40] L. J. Fernández-Alcázar, J. Lucas, R. A. Bustos-Marún, and H. M. Pastawski, Decoherence in current induced forces: Application to adiabatic quantum motors, Phys. Rev. B **92**, 075406 (2015).

[41] K. Bolotin, K. Sikes, Z. Jiang, M. Klima, G. Fudenberg, J. Hone, P. Kim, and H. Stormer, Ultrahigh electron mobility in suspended graphene, Solid State Commun. **146**, 351 (2008).

[42] K. I. Bolotin, K. J. Sikes, J. Hone, H. L. Stormer, and P. Kim, Temperature-dependent transport in suspended graphene, Phys. Rev. Lett. **101**, 096802 (2008).

[43] V. Singh, S. Sengupta, H. S. Solanki, R. Dhall, A. Allain, S. Dhara, P. Pant, and M. M. Deshmukh, Probing thermal expansion of graphene and modal dispersion at low-temperature using graphene nanoelectromechanical systems resonators, Nanotechnology **21**, 165204 (2010).

[44] L. Ma, J. Wang, and F. Ding, Recent progress and challenges in graphene nanoribbon synthesis, ChemPhysChem **14**, 47 (2013).

[45] Z. Zhang, X. Qi, J. Zhang, C. Guo, and Z. Zhu, Graphene-enabled electrically tunability of metalens in the terahertz range, Opt. Express **28**, 28101 (2020).

[46] T. Higuchi, C. Heide, K. Ullmann, H. B. Weber, and P. Hommelhoff, Light-field-driven currents in graphene, Nature (London) **550**, 224 (2017).

[47] X. Cong, Q.-Q. Li, X. Zhang, M.-L. Lin, J.-B. Wu, X.-L. Liu, P. Venezuela, and P.-H. Tan, Probing the acoustic phonon dispersion and sound velocity of graphene by Raman spectroscopy, Carbon **149**, 19 (2019).

[48] M. L. Polianski, M. G. Vavilov, and P. W. Brouwer, Noise through quantum pumps, Phys. Rev. B **65**, 245314 (2002).

[49] R.-P. Riwar, J. Splettstoesser, and J. König, Zero-frequency noise in adiabatically driven interacting quantum systems, Phys. Rev. B **87**, 195407 (2013).

[50] V. Balakrishnan, *Elements of Nonequilibrium Statistical Mechanics* (Springer, Cham, 2021).

[51] Y. Blanter and M. Büttiker, Shot noise in mesoscopic conductors, Phys. Rep. **336**, 1 (2000).

[52] C. J. Cattena, R. A. Bustos-Marún, and H. M. Pastawski, Crucial role of decoherence for electronic transport in molecular wires: Polyaniline as a case study, Phys. Rev. B **82**, 144201 (2010).

[53] L. J. Fernández-Alcázar, H. M. Pastawski, and R. A. Bustos-Marún, Nonequilibrium current-induced forces caused by quantum localization: Anderson adiabatic quantum motors, Phys. Rev. B **99**, 045403 (2019).

[54] M. Takamura, H. Okamoto, K. Furukawa, H. Yamaguchi, and H. Hibino, Energy dissipation in graphene mechanical resonators with and without free edges, Micromachines **7**, 158 (2016).

[55] J. Splettstoesser, M. Governale, J. König, and R. Fazio, Adiabatic pumping through a quantum dot with Coulomb interactions: A perturbation expansion in the tunnel coupling, Phys. Rev. B **74**, 085305 (2006).

[56] F. D. Ribetto, R. A. Bustos-Marún, and H. L. Calvo, Role of coherence in quantum-dot-based nanomachines within the Coulomb blockade regime, Phys. Rev. B **103**, 155435 (2021).

[57] D. S. Fisher and P. A. Lee, Relation between conductivity and transmission matrix, Phys. Rev. B **23**, 6851 (1981).

[58] N. Bode, S. Viola-Kusminskiy, R. Egger, and F. von Oppen, Current-induced forces in mesoscopic systems: A scattering-matrix approach, Beilstein J. Nanotechnol. **3**, 144 (2012).